Med Biol Eng Comput (2008) 46:701–707
DOI 10.1007/s11517-008-0332-0

ORIGINAL ARTICLE

Tensile radial stress in the spinal cord related to arachnoiditis or tethering: a numerical model

C. D. Bertram · L. E. Bilston · M. A. Stoodley

Received: 22 October 2007 / Accepted: 3 March 2008 / Published online: 18 March 2008

Abstract Spinal arachnoiditis comprises fibrous scarring of the subarachnoid space, following spinal trauma or inflammation, and is often associated with syringomyelia. We hypothesised that cord-to-dura attachments could cause transient tensile cord radial stress, as pressure waves propagate. This was tested in a fluid–structure interaction model, simulating three types of cord tethering, with 'arachnoiditis' confined to a short mid-section of the cord. The annular system was excited abdominally with a short transient, and the resulting Young and Lamb waves and reflections were analysed. Radial mid-section tethering was less significant than axial tethering, which gave rise to tensile radial stress locally when the cord was not fixed cranially. Simulated as inextensible string connections to the dura, arachnoiditis caused both localised tensile radial stress and localised low pressure in the cord as the transient passed. The extent of these effects was sensitive to the relative stiffness of the dura and cord. Tensile radial stress may create a syrinx in previously normal cord tissue, and transiently lowered pressure may draw in interstitial fluid, causing the syrinx to enlarge if fluid exit is inhibited. The suggested mechanism could also explain the juxtaposition of syrinxes to regions of arachnoiditis.

Parts of this work were presented at the 5th World Congress of Biomechanics, Munich, Germany, 29 July–4 August 2006, and at the Conquer Chiari Research Symposium, Chicago, USA, 2 June 2007.

C. D. Bertram (✉)
Biofluid Mechanics Laboratory, Faculty of Engineering,
University of New South Wales, Sydney 2052, Australia
e-mail: c.bertram@unsw.edu.au

L. E. Bilston · M. A. Stoodley
Prince of Wales Medical Research Institute, UNSW,
Barker Street, Randwick 2031, New South Wales, Australia

Keywords Fluid–structure interaction · Finite-element model · Cerebrospinal fluid · Wave propagation · Syringomyelia

1 Introduction

Syringomyelia is a condition where fluid-filled cavities (syrinxes) form within the spinal cord tissue. Syrinxes form in association with many spinal and cranio-spinal abnormalities, including spinal cord injury. Further spinal cord damage may result from syringomyelia, rendering a patient with a previous spinal cord injury even more incapacitated. Existing treatments for post-traumatic syringomyelia are unsatisfactory, with high recurrence rates. The lack of knowledge regarding the mechanism of syrinx formation is hindering the development of better treatments for this condition.

We have previously [1] developed fluid–structure interaction models of a simplified geometry for the spinal subarachnoid space (SAS), filled with cerebrospinal fluid (CSF), enclosing the spinal cord, bounded by the dura mater. Waves propagating in the system in response to excitation by transients of varying duration were investigated. Significant end-to-end pressure waveform differences existed only when the excitation was provided by transients shorter and sharper than arterial pulsation, such as percussive coughing, retching or sneezing. All these sources are essentially abdominal in origin, primarily generating cranially propagating waves.

Syrinx formation and location is often associated with arachnoiditis. In this study, we examine possible effects of localised tethering of the cord, as occurs with arachnoiditis. The cause of arachnoiditis may be spinal trauma, infection or inflammation (e.g., due to meningitis). Depending on

arachnoiditis severity, there may be several components, but the primary one is a degree of bonding of the cord to the dura. Three possible aspects of such tethering, radial constraint, axial constraint and string-like coupling of cord and dura, are examined. We find that tensile radial stress and lowered pressure (relative to starting or static values) in the cord tissue occur transiently at the level of arachnoiditis. We speculate that such tensile radial stress may play a role in the creation of a cavity in the cord, and that lowered pressure may draw extracellular fluid into the cavity and thus contribute to its enlargement.

2 Methods

2.1 Model geometry and properties

The geometry and properties of the overall model were largely as used previously [1]. The models were two-dimensional, axi-symmetric, fully coupled fluid–structure interactions realized in the finite-element software ADINA. The SAS was modelled as a tapered annulus, with dimensions chosen to match the average dimensions of the SAS in the Visible Human [14]; see Fig. 1. The spinal cord was an elastic solid, shaped as a tapered cylinder, prevented from moving axially at either the cranial end or the caudal end. The dura was a tapered elastic sleeve of constant thickness bounding the SAS, composed of stiffer material, prevented from axial motion at both ends. The CSF was given the properties of water and the solids were assumed linearly elastic for small deformations.

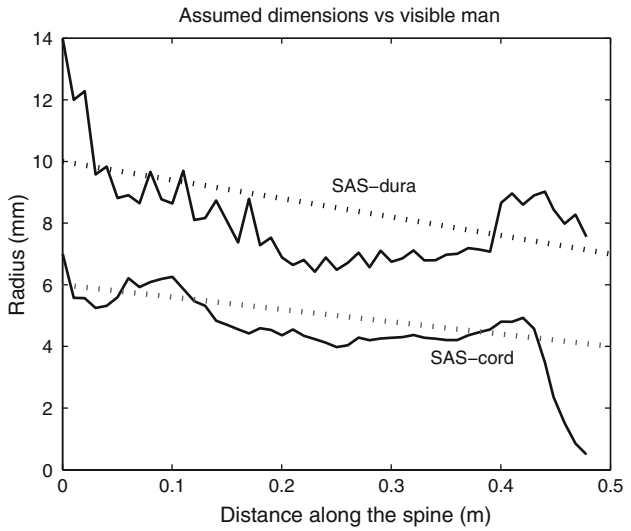

Fig. 1 Comparison of the dimensions of the subarachnoid space in the model (*dotted lines*) with data from the Visible Human Project® (*solid lines*). In this and other figures, distance is measured from the cranial end of the spinal cord. The cord and dura radii are slightly reduced from those used previously [1]

The model was excited by applying at the caudal end a triangular transient of total duration 5 ms and magnitude 100 Pa. This brief excitation was shorter than any likely physiological excitation (discussed below), but separated the response to the incident wave from the response to later reflections.

2.2 Viscoelastic properties

We chose the elastic modulus of the dura and of the cord to approximate the SAS wave-speed measured by MRI [7]. The Poisson ratio was set to 0.49. Two sets of viscoelastic conditions, termed V1 and V2, were investigated. To probe the effects of the ratio of cord and dura stiffness, the V1 dura modulus was halved and doubled, while leaving the cord stiffness unchanged.

A viscoelastic solid with decay functions was used, corresponding to a spring in parallel with series-spring/dashpot combinations. The material then had the characteristic equation

$$E = E_0 + E_1 \mathrm{e}^{-\beta_1 t} + \cdots + E_n \mathrm{e}^{-\beta_n t},$$

where E_i is the spring stiffness, β_i is the inverse time-constant for a spring/dashpot combination and $i = 1$ to n.

The V1 simulations were run in circumstances that gave rise to much artificial damping ('numerical viscosity'). Usefully, this attenuated the incident wave to the point where reflected waves were comparatively small, allowing the effects of the incident wave encountering a localised change in conditions to be examined largely in isolation. With this removed for V2, reflected waves tended to dominate the responses. The extent of reflection was felt to be largely artefactual, as discussed below. Therefore, the V2 viscoelastic properties of the solids were chosen to give maximal energy dissipation, after restoration of the wave-speed. The parameter values are shown in Table 1. Which viscoelastic conditions were employed for each run is indicated in the figure captions.

2.3 Tethering zone

A short mid-section of the cord, 0.225–0.250 m from the cranial end, was defined as a separate entity. The cell vertices on the side facing the SAS were either unconstrained, prevented from motion in the y-direction (radial

Table 1 Values of viscoelastic parameters

	E_0 (MPa)		Decay functions, cord/dura		
	Cord	Dura	n	E_i (MPa)	β_i (s^{-1})
V1	0.125	2.5 (or 1.25, or 5)	3	E_0	$100i$
V2	0.0625	1.25	1	$2E_0$	2,000

tethering), or prevented from motion in the z-direction (axial tethering).

The third type of tethering examined was by joining this mid-section of the cord to the dura by six equi-spaced spring elements, which were sufficiently stiff in tension to be effectively inextensible, and had zero compressive stiffness. These strings did not interact with the fluid model, except insofar as they locally changed the boundaries of the SAS. It was found that they pulled the cord cell vertices to which they were attached outwards locally, so that each string caused a pronounced separate maximum of cord radius. To limit this tendency and to model surface fibrosis on the cord, a 'crust' of the outer 20% of the cord radius was defined by further subdivision of the numerical surface for the cord. The thickness of this crust was 0.8 mm at the caudal end of the model and 1.2 mm at the cranial end, tapering linearly between these extremes in proportion to the rest of the cord radius. In the arachnoiditis region only, the crust had the same viscoelastic properties as the dura; elsewhere, it was not distinguished from the rest of the cord.

3 Results

We present the results by (1) plotting selected stress variables along a model boundary, usually the axis of symmetry or the cord–SAS interface, at selected times, and (2) showing solid model outlines at selected times, with deflections exaggerated.

3.1 Radial and axial tethering

Localised midpoint axial tethering had stronger effects on cord displacement than equally localised radial tethering. Animations of the model outline with exaggerated deflections showed that when the tethered section was allowed to move axially, the Young wave was able to pass through without losing its character. The cord lengthened in accommodating the Young wave, in the process moving the tethered mid-section cranially. Simultaneously, the dura shortened, but much less so. In contrast, radial mid-section tethering caused the wave to 'pile up' in front of the tethered part, which moved very little axially despite being free to do so. Instead, the Young wave was substantially reflected, and a much reduced wave was transmitted onward. The cord still lengthened, but less so than when the mid-section was untethered or axially tethered. For all of these runs, the model cord was free to move axially at the cranial end, but secured at the caudal end.

Thus, with the cord anchored caudally, axial mid-section tethering led to transiently positive radial stress just downstream of the tethering. With axial tethering, the zone of positive radial stress both extended further lengthwise and lasted longer than when tethering was radial or absent. However, simulation of axial mid-point tethering with the cord anchored at the cranial end instead (the more realistic situation) showed almost no tensile radial stress.

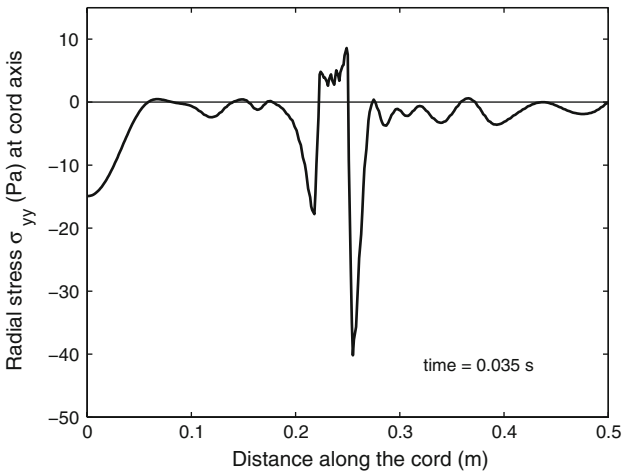

Fig. 2 Profile of radial stress in the cord (condition V2) as a function of axial position, 35 ms after the start of excitation, on the cord axis of symmetry

3.2 Dura-to-cord strings

For these simulations, the cord was again anchored at the cranial end and free to move axially at the caudal end. When waves passed which tended to compress the cord and expand the dura, the inextensible links between the inner surface of the dura and the outer surface of the cord created a localised zone of radial tension in the cord. Figure 2 shows radial stress in the cord on the axis of symmetry. Peaks of radial stress (not shown) occur closer to the cord surface at the locations of the six equispaced strings. The time is when the Young wave was centred on the zone of the strings. On the cord axis, there is a continuous zone of tensile stress, which is highly localised to the string region. This is crucial: the length of the radially tensed zone is determined by the arachnoiditis, not by the wavelength.

The zone of radial tension was also where negative pressure[1] occurred in the cord tissue. Negative here means less than the static and spatially uniform pre-existing value in the absence of all wave activity. The existence of tensile radial stress and negative cord tissue pressure was affected by the relative stiffness of the model dura and cord.

[1] The concept of pressure here requires careful definition, since strictly there are only directed stresses in an elastic solid. Pressure is calculated as minus the average of the mutually orthogonal normal stresses. If the solids were microporous, with a fluid content component (as it is in reality in the case of cord tissue), the fluid would have this pressure.

Figure 3 shows the effect of doubling or halving the elastic stiffness of the dura on cord axis pressure; our interest is in whether the pressure ever becomes negative. As seen in Fig. 3a, the dura/cord stiffness ratio substantially affects the overall progress of the transient; the wave arrives sooner when the dura is stiffened and there is less attenuation. Figure 3b shows a later time, during the subsequent reflections of the incident pulse, and concentrates on the vicinity of the strings. The time is when the control conditions yield the greatest negative pressure. At this time the stiffened dura causes a larger zone of greater negative pressure (slightly earlier times would have shown still more negative pressure). With the weakened dura, there is no negative pressure at this time, and negative pressures were scarcely reached at any time during the dissipation of the transient.

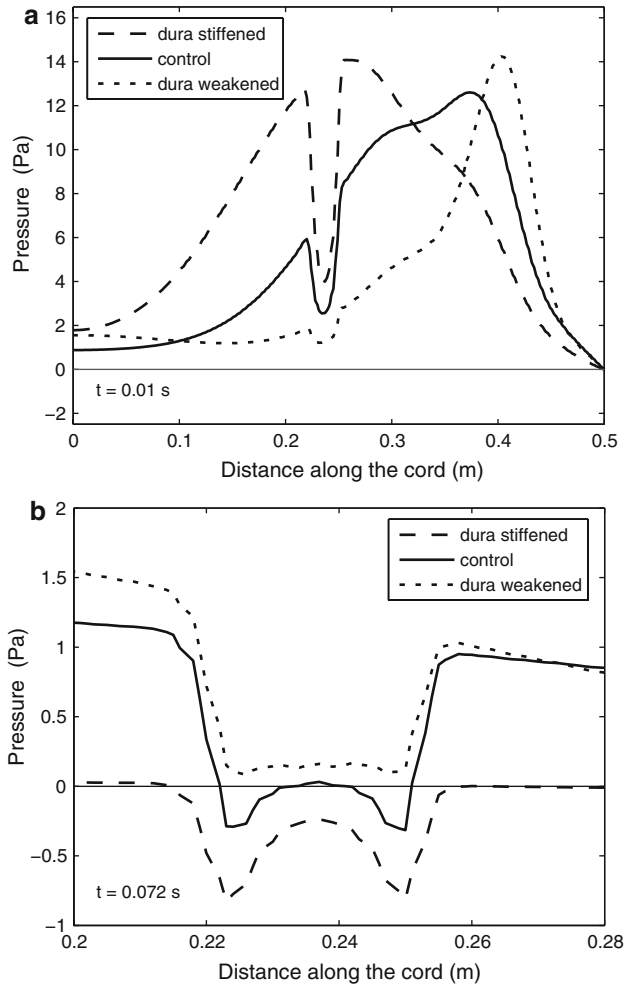

Fig. 3 Variation of the ratio of dural stiffness to cord stiffness. Profiles of cord-axis pressure versus distance along the cord (condition V1). *Solid line* baseline ratio, *dashed line* dural material twice as stiff, *dotted line* dural material half as stiff. **a** Whole cord, 10 ms after the start of caudal excitation. **b** String neighbourhood, 72 ms after excitation

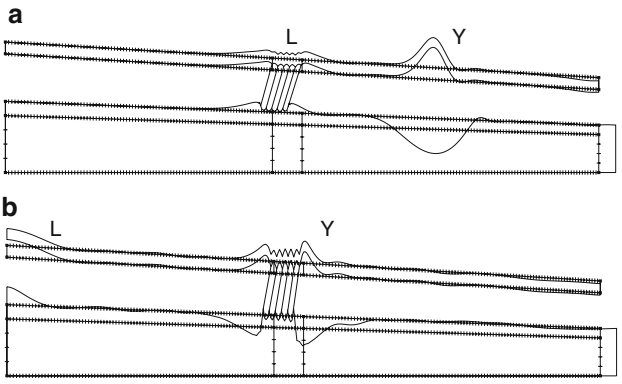

Fig. 4 The deflection of the model with cord/dura strings at two different times, **a** 20 ms and **b** 35.5 ms, after the initiation of the caudal (right-hand end) transient (condition V2). To make the deflections visible, they are exaggerated by a factor of 2,500. The original position of the model is also shown. The model extends radially from an axis of 2D axi-symmetry at the bottom of each panel; the radial dimensions are here magnified relative to the axial ones by a factor of 10

The excitation creates both a Young wave and a Lamb wave, which propagates twice as fast. Both waves pass the string region essentially unchanged and are reflected at the cranial end without inversion. The differing nature of the Lamb and Young waves is illustrated in Fig. 4, which shows the model outline at two instants during the early propagation of the incident waves. In Fig. 4a, the Lamb wave (labelled L) has reached the zone of string attachments, while the Young wave (labelled Y) is still making its way along the caudal half of the SAS; in Fig. 4b, the Young wave (Y) is centred on the string region, while the Lamb wave (L) has reached the cranial end. The Young wave is more obvious: as a localised increase of pressure in the SAS, it distends the dura and compresses the cord, which lengthens caudally as a result. When it reaches the strings, their inextensibility causes the distended dura to be locally pulled inwards, transmitting tension to the cord, which is locally pulled outwards to the point where it regains or exceeds its original radius. This is the mechanism by which tensile radial stress and negative pressure are generated in the cord material as the wave passes.

The Lamb wave compresses the cord material axially. Since the material is essentially incompressible, the compression causes radial expansion (Fig. 4a), which is then transmitted to the dura by the inertia of the fluid in the SAS. Radial expansion is minimal in the string region, because of the stiffened cord crust. Via tension in the strings, the dura is then also pulled inwards locally by the cord crust, relative to the position it would otherwise adopt under the influence of the wave. Referring to Fig. 4b, this is also why the cord outside radius is so close to its original value in the string region as the Young wave passes. The

crust resists both the radial compression and the axial lengthening that the Young wave otherwise causes.

The Lamb wave does *not* produce radial cord tensile stress, despite an increase in cord radius. The cord is under axial compression, and there is associated radial expansion, but this is not accompanied by tensile radial stress (result not shown). In contrast, the passage of the Young wave a little later does create radial tensile stress in the cord at the site of the 'arachnoiditis'.

4 Discussion

This study has shown that, under certain circumstances, arachnoiditis could lead to transiently negative pressures and radial tensile stresses in the spinal cord underlying the arachnoiditis. Further experimental and modelling research may be able to determine the role this might play in syrinx development.

Syringomyelia occurs secondary to a wide array of disorders affecting the spine and craniocervical junction. Syrinxes form in the central canal of the cord (canalicular syrinxes) or in the cord tissue separate from the central canal (extracanalicular). The mechanism of formation of each type may be different. Like most research, this study has focussed on possible hydrodynamic theories to explain syrinx development, although other mechanisms may also be involved. For example, Levine [9] has suggested a mechanism related to disruption of the blood–brain barrier by mechanical stresses on the cord. The present study is particularly relevant to post-traumatic, infectious or inflammatory syringomyelia, with which arachnoiditis is associated. We have concentrated on localised arachnoiditis; this condition can also be extensive along the spine and is then associated with considerable impediment to CSF motion, here assumed negligible. Other situations where localised tethering occurs include diastematomyelia and thickened filum.

4.1 Limitations of the model

In considering the results, the many limitations and simplifications of the model must be borne in mind. First, the geometry is axi-symmetric. While for the physiological spinal cord this is fairly realistic, it is unlikely that any pathological change such as localised arachnoiditis secondary to trauma will be as symmetrical. The concept of axi-symmetric strings has no physical equivalence; the best approximation would be strings spaced rather closely around the cord circumference.

Axi-symmetry combined with isotropy also produced a collar effect when the surface of the cord was locally stiffened where the arachnoid 'strings' inserted. This limited the extent to which waves could locally affect the cord diameter, and therefore caused increased reflection. Since only the axial and radial directions are defined in an axi-symmetric model, specifying different circumferential and axial stiffnesses for the stiffened cord surface was not possible. This would require a three-dimensional model. The collar is however an effective model of another not uncommon result of arachnoiditis, the calcification of the pia mater.

Since the model is linear, the specific magnitudes of the excitations and resulting deflections, pressures and stresses are relatively unimportant. We have taken an excitation magnitude of 100 Pa (about 0.75 mmHg), as suggested by the results of Heiss et al. [8]. This magnitude relates to cardiac-induced SAS pressure changes, as a result of displacement of CSF from the skull during cranial arterial systole. Williams [18] recorded SAS pressure changes in the lumbar region of the order of 75 mmHg or more, arising from coughing in the sitting position. In the linear model, such a hundred-fold increase in excitation magnitude would proportionately increase the magnitudes of all response quantities.

A further weakness of our model is the over-dominance of wave reflections. The extent of reverberation, when artificial damping was removed, is an artefact caused by the simplicity of the geometry. Where in our model the SAS was a smooth-walled space (except where we defined 'arachnoiditis'), in reality it contains nerves, trabeculae and denticulate ligaments [13]. Together with irregularities in the surfaces of the dura mater and the pia mater, these structures would cause more rapid wave attenuation than we observed numerically. However, the major cause of reverberation in the model is undoubtedly the unphysiologically large wave reflection at each end, where the model ends abruptly but the hindbrain and cauda equina would normally absorb waves. This could be addressed in future studies.

4.2 Comparison of elastic properties with real ones

The materials of the cord and dura are assumed in the model to be both linear and isotropic, and there is experimental evidence that neither of these simplifications is justified. Moreover, the cord tissue is porous, with a high fluid content, so much so that in the absence of the confining pia mater membranous sheath it is scarcely solid at all [4].

The model does not incorporate anisotropy for either the cord or the dura, although there is experimental evidence that the dura is stiffer longitudinally than circumferentially [12]. Measured Young's moduli vary widely (e.g., 65–103 MPa longitudinally, 4–8 MPa circumferentially for human lumbar dura [12]; 0.4 MPa at a strain of 0.14, rising to 46 MPa at strain 0.18 for canine thoraco-lumbar dura

[15]). The values used here are at the lower end of those reported, appropriate for an operating point at a physiologically low SAS pressure. The picture is similar for the spinal cord, which is again anisotropic and nonlinear. Also, the cord parenchyma is very much softer than the thin pia mater encasing it [10, 11]. Again based on low strain, we have chosen a value for the cord modulus towards the low end of the range in the literature (e.g., 520–1,880 kPa at strain rates of 0.04–0.24 s^{-1} for human cord with pia mater attached [2]; 1,400 kPa, dropping to 89 kPa when the pia mater was removed, at rates of 1 and 10 s^{-1} [10]), and have not specified the pia mater separately. Differing ways of reporting measurements of time-dependent dural elastic properties [6, 16, 17] make their comparison problematic, and comparison with the values assumed here is not attempted.

4.3 Postulated mechanism

We previously [1] explored the basics of wave propagation in the limited-length annular fluid space of the SAS bounded inside by the cord and outside by the dura.[2] Here, we have added to our model three different possible attributes arising from localised tethering by arachnoiditis. Our results indicate that 'pure' radial and axial tethering of the cord do not lead to either tensile radial stress or transiently lowered hydrostatic pressure in the cord tissue when the cord is free to move at the caudal end.

Rather more intriguing behaviour was found when arachnoiditis was modelled as inextensible strings between the cord and dura. Although radial cord motion was limited by the stiffened cord surface, which we introduced to spread the effects of the string insertions, we found both tensile radial stress and transiently lowered pressure in the cord material. It is possible that repeated transients of tensile radial stress may produce a syrinx in previously healthy cord tissue and/or that transiently lowered hydrostatic pressure, corresponding physiologically to pressure in the interstitial space, may contribute to the subsequent enlargement of such a syrinx. We suggest that the hypothesis should be further investigated both experimentally and numerically.

The magnitude of the tensile stress found is very much less than the elastic modulus of the cord, and is thus unlikely to substantially damage the cord on its own. However, the transverse strength of spinal cord tissue in tension has not been measured, and traumatised spinal cord may be weaker than healthy cord. As shown by Ozawa et al. [11], cord tissue without the pia is very weak, and transverse strength in tension may be substantially lower than axial tensile strength.

Transiently lowered pressure in a local part of the cord is insufficient alone to accumulate interstitial fluid in a syrinx. If either cyclic events such as arterial pulsation or occasional ones such as coughing are to produce chronic engorgement of a cavity, there must in addition be a mechanism for the one-way travel of fluid; egress must be harder than entry. Our hypothesis does not directly address this issue. Thinking more of transiently raised SAS pressure than lowered cord tissue pressure, Bilston et al. [3] have postulated that flow from the SAS to the interior of the cord tissue may be encouraged by pulsatile distension of the microscopic arteries around which the perivascular spaces provide a channel for CSF transport into the cord.

In summary, this study has shown that, under the right circumstances, it is possible for arachnoiditis that results in tethering of the cord to give rise to localised regions of lowered pressure and tensile radial stress adjacent to the tethered region. This postulated new mechanism may contribute to syrinx formation and/or enlargement in the presence of arachnoiditis. Further work is needed to determine the significance of these effects in physiologically realistic conditions.

[2] Further analysis of wave propagation in an infinitely long annular space bounded outside by a rigid conduit and inside by an elastic vessel containing another fluid is given by Cirovic et al. [5], particularly for Young waves. They also analyse a model consisting of two coaxial solid elastic annuli creating three coaxial fluid spaces within a rigid outermost tube.

References

1. Bertram CD, Brodbelt AR, Stoodley MA (2005) The origins of syringomyelia: Numerical models of fluid/structure interactions in the spinal cord. ASME J Biomech Eng 127:1099–1109
2. Bilston LE, Thibault LE (1996) The mechanical properties of the human cervical spinal cord in vitro. Ann Biomed Eng 24:67–74
3. Bilston LE, Fletcher DF, Brodbelt AR, Stoodley MA (2003) Arterial pulsation-driven cerebrospinal fluid motion in the perivascular space: a computational model. Comput Methods Biomech Biomed Eng 6:235–241
4. Carpenter PW, Berkouk K, Lucey AD (2003) Pressure wave propagation in fluid-filled co-axial elastic tubes, part 2: Mechanisms for the pathogenesis of syringomyelia. ASME J Biomech Eng 125:857–863
5. Cirovic S, Walsh C, Fraser WD (2002) Wave propagation in a system of coaxial tubes filled with incompressible media: a model of pulse transmission in the intracranial arteries. J Fluids Struct 16:1029–1049
6. Galford JE, McElhaney JH (1970) A viscoelastic study of scalp, brain, and dura. J Biomech 3:211–221
7. Greitz D, Ericson K, Flodmark O (1999) Pathogenesis and mechanics of spinal cord cysts—a new hypothesis based on magnetic resonance studies of cerebrospinal fluid dynamics. Int J Neuroradiol 5:61–78
8. Heiss JD, Patronas N, DeVroom HL, Shawker T, Ennis R, Kammerer W, Eidsath A, Talbot T, Morris J, Eskioglu E, Oldfield EH (1999) Elucidating the pathophysiology of syringomyelia. J Neurosurg 91:553–562

9. Levine DN (2004) The pathogenesis of syringomyelia associated with lesions at the foramen magnum: a critical review of existing theories and proposal of a new hypothesis. J Neurol Sci 220:3–21
10. Mazuchowski EL, Thibault LE (2003) Biomechanical properties of the human spinal cord and pia mater. In: ASME summer bioengineering conference, Key Biscayne, Florida, 25–29 June 2003, pp 1205–1206
11. Ozawa H, Matsumoto T, Ohashi T, Sato M, Kokubun S (2004) Mechanical properties and function of the spinal pia mater. J Neurosurg Spine 1:122–127
12. Runza M, Pietrabissa R, Mantero S, Albani A, Quaglini V, Contro R (1999) Lumbar dura mater biomechanics: experimental characterization and scanning electron microscopy observations. Anesth Analg 88:1317–1321
13. Stockman HW (2006) Effect of anatomical fine structure on the flow of cerebrospinal fluid in the spinal subarachnoid space. ASME J Biomech Eng 128:106–114
14. The visible human project®: U.S. National Library of Medicine. http://www.nlm.nih.gov/research/visible/visible_human.html
15. Tunturi AR (1977) Elasticity of the spinal cord dura in the dog. J Neurosurg 47:391–396
16. Tunturi AR (1980) Viscoelasticity of dog spinal cord. Physiol Chem Phys 12:373–378
17. Wilcox RK, Bilston LE, Barton DC, Hall RM (2003) Mathematical model for the viscoelastic properties of dura mater. J Orthop Sci 8:432–434
18. Williams B (1976) Cerebrospinal fluid pressure changes in response to coughing. Brain 99:331–346